RSC Sustainability

ROYAL SOCIETY OF CHEMISTRY

PAPER

View Article Online
View Journal

Cite this: DOI: 10.1039/d5su00947b

Enhanced plant growth and harvestable yield through fluorescent copper-based composites

Konstantinos T. Kotoulas,[abc] Thomas Hinton,[a] Ethan Macallister,[a] Jai Ram,[a] John D. Wallis,[c] Yunhong Jiang,[d] Andrew D. Burrows,[b] Gareth W. V. Cave[d] and Ming Xie*[a]

Improving crop productivity without increasing land, energy or chemical inputs is a critical challenge for sustainable agriculture, and spectral conversion materials that transform underutilized ultraviolet radiation into photosynthetically active radiation (PAR) offer a promising solution. Here, we report copper-based luminescent composites that enable wavelength-selective spectral reshaping and evaluate their physiological impact on *Raphanus sativus* grown under controlled greenhouse conditions. Three complementary materials were developed: melt-quenched glass composites incorporating the copper iodide clusters $[Cu_4I_4(PPh_3)_4]$ and $[Cu_4I_4(PPh_2Et)_4]$, and flexible cellulose acetate films embedded with copper-carbon nanoassemblies (Cu-CNAs), producing blue-green, yellow, and blue emissions, respectively, within the PAR window. Plant trials revealed clear wavelength dependent responses, with blue and blue-green emission accelerating early foliar expansion, while prolonged exposure to the yellow emitting $[Cu_4I_4(PPh_2Et)_4]$ composite delivered the highest final biomass and significantly increased chlorophyll, carotenoid and ascorbic acid content, indicative of enhanced carbon assimilation and photoprotective metabolism. These results demonstrate that copper-based luminescent composites provide a scalable, low-cost and sustainable platform for spectral optimization in controlled environment agriculture, offering a practical materials driven strategy to improve both crop yield and nutritional quality.

Received 23rd December 2025
Accepted 3rd April 2026

DOI: 10.1039/d5su00947b

rsc.li/rscsus

Sustainability spotlight

This work advances sustainable agriculture by enabling yield and nutritional gains without increasing land use, fertiliser inputs, or energy demand. Copper-based luminescent composites convert underutilised and potentially harmful UV radiation into photosynthetically active wavelengths, improving photosynthetic efficiency, biomass accumulation, and micronutrient content under controlled growth conditions. The materials are low-cost, scalable, and based on earth-abundant copper, offering a lower environmental footprint than rare-earth or precious-metal phosphors. By enhancing crop productivity through passive spectral optimisation, this research supports SDG 2 (Zero Hunger), SDG 12 (Responsible Consumption and Production), and SDG 13 (Climate Action), contributing to resilient, resource-efficient food production systems.

1 Introduction

With the global population expected to approach 10 billion by 2050, agricultural productivity must increase by approximately 50% to meet rising food demand. This challenge is exacerbated by constraints in arable land, rising energy costs, and environmental concerns associated with conventional agricultural intensification. Enhancing the efficiency of photosynthesis presents a promising route to achieving higher crop yields while reducing the environmental footprint of food production.[1]

Photosynthetically active radiation (PAR; 400–700 nm) is the range of light most efficiently absorbed by chlorophylls and carotenoids for driving photosynthesis.[2] However, a significant fraction of incoming solar radiation lies outside this range, particularly in the ultraviolet (UV) region, which can be photodamaging and is poorly utilized by plants.[3,4] Materials that harvest UV light and convert it into red, blue, or green light can enhance the photon flux in spectral regions most relevant to photosynthesis, thereby improving photosynthetic efficiency.

Red light (650–700 nm) is particularly efficient in stimulating CO_2 fixation,[5,6] while blue light (450–490 nm) supports chlorophyll biosynthesis and photomorphogenic development through cryptochrome activation.[7,8] Green light, once considered inefficient, has been shown to penetrate deeper into leaf mesophyll layers, promoting photosynthesis in tissues not reached by red or blue light, improving drought tolerance and growth rate.[9,10] A balanced spectral profile incorporating all

[a]Department of Chemical Engineering, University of Bath, Bath, BA2 7AY, UK. E-mail: m.xie2@bath.ac.uk
[b]Department of Chemistry, University of Bath, Bath BA2 7AY, UK
[c]School of Science and Technology, Nottingham Trent University, Nottingham, NG11 8NS, UK
[d]Department of Applied Sciences, Northumbria University, Newcastle NE1 8ST, UK

three wavelengths is essential for optimal plant development and avoiding phenomena such as "red light syndrome", which can reduce pigment production and leaf health when plants are grown under monochromatic red light alone.[2]

Copper nanoclusters (Cu-NCs) and copper halide-based materials offer a sustainable and tuneable approach to spectral conversion.[11] Cu-NCs exhibiting strong photoluminescence, are water-soluble, less toxic and more economical to produce, with a lower environmental impact than alternative precious metal nanoparticle (Au, Ag) approaches and or lanthanide-based phosphors.[12,13] In addition, these materials can be integrated into polymeric films (*e.g.* cellulose acetate) or immobilized within inorganic glass matrices to create luminescent coatings and filters that convert UV radiation into PAR wavelengths.

In this study, we detail the development of copper-based fluorescent composites, including melt-quenched copper phosphine halide complexes and polymer films containing Cu-NCs that convert harmful UV radiation into beneficial yellow, blue, or green light. These materials are designed for integration into greenhouse environments or as leaf-adjacent films to modulate the incoming light spectrum and enhance photosynthetic performance.

2 Materials and methods

Copper-based nanomaterials were synthesised and incorporated into spectral-converting composites for plant trials. $[Cu_4I_4(PPh_2Et)_4]$ and $[Cu_4I_4(PPh_3)_4]$ complexes were prepared *via* ligand-CuI complexation in a synthesis modified from previous literature.[14] The copper iodide complexes were melt-quenched onto polymethyl methacrylate sheets, whilst polyvinylpyrrolidone-stabilised copper nanoassemblies were incorporated into cellulose acetate films for spectral conversion studies.

2.1 Chemicals

Anhydrous copper(II) chloride (99.0%) was purchased from Acros Organics. Ethyldiphenylphosphine (97.0%) was obtained from Tokyo Chemical Industry UK Ltd. Cellulose acetate (Mw ≈ 30 000), copper(I) iodide (98.0%), polyvinylpyrrolidone (PVP, 99.0%), potassium phosphate (99.0%), diethyl ether (Et_2O, 97.5%), triphenylphosphine (PPh_3, 98.5%), phosphoric acid (H_3PO_4, 85.0%), potassium chloride (KCl, 99.0%), potassium hydroxide (KOH, 85.0%), sodium phosphate dibasic (99.0%), triethyl amine (TEA, 99.5%), ethyl acetate (EtOAc, 99.5%), and sodium phosphate monobasic (99.0%) were all purchased from Sigma-Aldrich. Chloroform (99.8%), ethanol (EtOH, 99.0%) and hydrochloric acid (HCl, 37.0, were obtained from Fisher Scientific UK. Acetone (99.0%) and methanol (MeOH, 99.5%) were sourced from VWR Chemicals. All aqueous solutions were prepared using distilled water from an ELGA PURELAB Option-S 15BP benchtop water purification system (18.2 MΩ cm).

2.2 Syntheses of copper nanoclusters and nanomaterials

2.2.1 Synthesis of $[Cu_4I_4(PPh_3)_4]$ and $[Cu_4I_4(PPh_2Et)_4]$ nanoclusters and glass composites. The synthesis of copper(I) iodide nanoclusters was modified from previous literature.[14] Two variants were prepared using either triphenylphosphine (PPh_3) or ethyldiphenylphosphine (PPh_2Et) ligands. In both cases, copper(I) iodide (10.50 mmol, 2.00 g) was added to a round-bottom flask containing chloroform (60.00 mL) and stirred for 24 hours at room temperature under an argon atmosphere. For the PPh_3 complex, triphenylphosphine (30.50 mmol, 8.00 g) was used; for the PPh_2Et variant, ethyldiphenylphosphine (18.70 mmol, 4.00 g) was employed. After the reaction, diethyl ether (20 mL) was added to precipitate white crystals with yields based on copper of 58% and 61% for PPh_2Et and PPh_3 complexes respectively. The purified nanoclusters were then subjected to melt-quenching at 290 °C in a Lenton Thermal Designs EF 11/8B muffle furnace, forming glass composites on 2 mm thick PMMA substrates. PMMA was specifically selected for its high transparency (typically >90%) across the photosynthetically active radiation (PAR; 400–700 nm) region.

2.2.2 Synthesis of copper doped carbon nano assemblies (Cu-CNAs). Copper(II) chloride (1.49 mmol, 0.20 g) and polyvinylpyrollidone (1.80 mmol, 0.20 g) were dissolved in deionised water (20 mL) before being transferred to a 100 mL polytetrafluoroethene (PTFE) solvothermal autoclave reactor and were heated at 200 °C and 10 bar for 5 hours in a Memmert U Universal oven. After cooling, the resulting green solution was passed through a millex PTFE syringe filter (0.20 μm pore size) before being dried (60 °C overnight) to a powder prior to plant trials.

2.2.3 Synthesis of cellulose acetate composite films. Cellulose acetate (24.30 mmol, 7.00 g) was dissolved in acetone (200 mL) under continuous stirring. The resulting solution was degassed using both an Ulsonix Proclean 1560 sonicator and a Thermo Scientific Vacutherm Series Model VT 6025 vacuum oven at room temperature to remove trapped air. For composite preparation Cu-CNAs (0.30 g) were added to the degassed polymer solution and stirred overnight (500 rpm) to ensure uniform dispersion. The resulting mixture was then cast slowly into a glass dish and dried at 60 °C for 12 hours, yielding a yellow tinted film. Cellulose acetate was selected due to its high optical transparency in the visible range, with the tint coming from the nanomaterials embedded.

2.3 Characterisation

2.3.1 Scanning electron microscopy (SEM). Prior to analysis, samples were coated in chromium (10 nm). A field emission scanning electron microscope (JSM-7900 F, JEOL, Japan) was used to observe the surface morphologies of the cellulose acetate films. To track the Cu-NCs, a field emission scanning electron microscope (SU3900, HITACHI, Japan) with an Energy Dispersive X-ray analyser (EDX) attached (Oxford Instruments Ultim Max 170 mm^2) was used to confirm the presence of copper.

2.3.2 Single crystal X-ray diffraction (SCXRD). Molecular structures of a new polymorph of $[Cu_4I_4(PPh_2Et)_4]$ and previously reported $[Cu_4I_4(PPh_3)_4]$ were obtained by crystals grown from slow evaporation (chloroform:diethyl ether, 3 : 1. X-ray diffraction data were collected on a Rigaku XtaLAB Synergy-DW diffractometer using MoKα radiation at 140 K for the ethyldiphenylphosphine complex, and CuKα radiation at 120 K for the triphenylphosphine complex. The structures were solved with SHELXT,[15] and refined with SHELXL,[16] using the OLEX2 program.[17] Illustrations were made with MERCURY.[18]

2.3.3 Fluorescence spectroscopy. Fluorescence excitation and emission measurements were performed using an Agilent Cary Eclipse Fluorescence Spectrophotometer, and a Hellma Analytics quartz cuvette (1 cm path length). Spectra were collected over a range of 1100–200 nm, using a scan step size of 2 nm and 25 excitation/emission slits.

2.4 Plant cultivation

Raphanus sativus (Radish F1) was grown in an AutoPot® passive watering setup using four AutoPot 8.5 L pots, (25 cm × 25 cm), each containing eight biological replicates $n = 8$ This was done in a Biobizz light mix soil ($N = 100$ mg L^{-1}, $P = 100$ mg L^{-1}, $K = 150$ mg L^{-1}) with no additional nutrients supplied to the plants. Plants were cultured in a greenhouse for 32 days using ambient light supplemented with a Daylight Maxibright 480 W/660 W LED grow light, with three additional Maxibright Daylight LED UV-A and UV-B bars at 60 W which came on six times a day for 10 minutes at 2 hour intervals (22 ± 2 °C, 138.71 ± 3.10 μmol m^{-2} s^{-1}, 12 hours light/12 hours dark photoperiod). Pot 1 was used as a control study for the three other pots. Pot 2 was grown under an $[Cu_4I_4(PPh_2Et)_4]$ glass/PMMA filter composite. Pot 3 was grown under a $[Cu_4I_4(PPh_3)_4]$ glass/PMMA filter composite. Pot 4 was grown under the cellulose acetate film containing Cu-CNAs). While this design emphasizes plant-level variance within a specific spectral environment, we acknowledge the potential for pot-specific effects.

Throughout the trials, plant foliage area was monitored at different stages of the trial and quantified using ImageJ software. Post harvest, the crops were weighed and then lyophilized, under a vacuum (<5 Pa) at a condenser temperature of −71.8 °C.

2.5 Quantification of plant nutrient profile

2.5.1 Ascorbic acid content. Powdered *Raphanus sativus* root tissue was added to a phosphate buffer: chloroform mixture (15 mL, 75 : 25) and agitated under dark conditions (room temperature for 24 h). The phosphate buffer (1 L) consisted of 25 mL of 1 M KOH (25 mL, 1 M),1 M phosphoric acid (30 mL, 1 M), and methanol (100 mL, HPLC grade). After 24 h, the mixture was centrifuged (7000 rpm, 10 minutes) using an Eppendorf 5418 R centrifuge, and the aqueous phase was collected and filtered through a syringe filter (0.22 μm). Ascorbic acid content was quantified using an Agilent 1290 Infinity II HPLC system with a diode-array detector (DAD). Separation was performed on a Restek Raptor C18 column (2.7 μm particle size, 100 mm length, 4.6 mm diameter), using phosphate buffer as the mobile phase (0.3 mL min^{-1} flow rate, 2 μL injection volume). Detection was monitored at 210 and 265 nm.

2.5.2 Chlorophyll and carotenoid extraction and quantification. Chlorophyll and carotenoid contents were determined using a standard method. Crop foliage samples were extracted in acetone: anhydrous ethanol mixture (20 mL of a 1 : 1 v/v) and incubated in the dark (room temperature, 24 h). Following extraction, the supernatant (0.1 mL) was transferred into a Hellma Analytics quartz cuvette (1 cm path length) and diluted to a final volume of 3 mL with the same solvent mixture.

Absorbance measurements were recorded at 440, 645, and 663 nm using an Agilent Cary 60 UV-vis spectrophotometer to quantify the concentrations of chlorophyll a, chlorophyll b, and total carotenoids (SI eqn (S1)–(S4)).

2.6 Statistical analys

All quantitative data are expressed as the mean ± standard deviation (SD) of $n = 8$ biological replicates per treatment. Statistical significance between each experimental treatment and the control group was determined using two-tailed, heteroscedastic (Welch's) *t*-tests to account for potential unequal variances between groups. Normality of the data was assumed based on the biological nature of the samples. All statistical calculations were performed using Microsoft Excel, and exact *p*-values are reported where applicable. A *p*-value of <0.05 was considered statistically significant.

3 Results and discussion

3.1 Copper iodide complexes enable UV-to-visible light conversion

The tetragonal $[Cu_4I_4(PPh_2Et)_4]$ polymorph crystallised from the slow evaporation of chloroform/diethyl ether as large colourless blocks, in contrast to the known orthorhombic polymorph which produced much smaller crystals from the same solvent system (Fig. 1) (14). The space group is I-4, and only one quarter of the molecular structure of the functionalised Cu_4I_4 cube is crystallographically unique, since it lies on a four-fold rotoinversion axis. The Cu–I bond lengths (2.6722(11), 2.6794(11) and 2.7669(12) Å) and I–Cu–I angles (97.80(3), 103.37(4) and 105.99(4)° are comparable and suggest no chemical difference those observed in the orthorhombic polymorph where half the molecule is crystallographically unique (2.678–2.721 Å, 98.03 & 98.62, 103.88, 106.51, 107.20 & 107.31°). The Cu–I–Cu angles (73.67(3), 75.22(4) & 78.55(3)°) are also similar to those in the orthorhombic polymorph (71.91–77.34°). For $[Cu_4I_4(PPh_3)_4]$ a monoclinic cell with dimensions $a = 13.4235(1)$, $b = 26.4678(3)$, $c = 19.4357(2)$ Å, $\beta = 99.282(1)°$ was found, and the structure solved satisfactorily to a *R* value of 0.0251 (Fig. 1).

The two copper iodide complexes were melt quenched, to produce fluorescent coatings that were then applied to polymethyl methacrylate planes for greenhouse applications, yielding blue and yellow fluorescence under 365 nm excitation for $[Cu_4I_4(PPh_3)_4]$ and $[Cu_4I_4(PPh_2Et)_4]$ respectively (Fig. 1). The emission characteristics of the melt-quenched glass composites were assigned based on the structural match between our

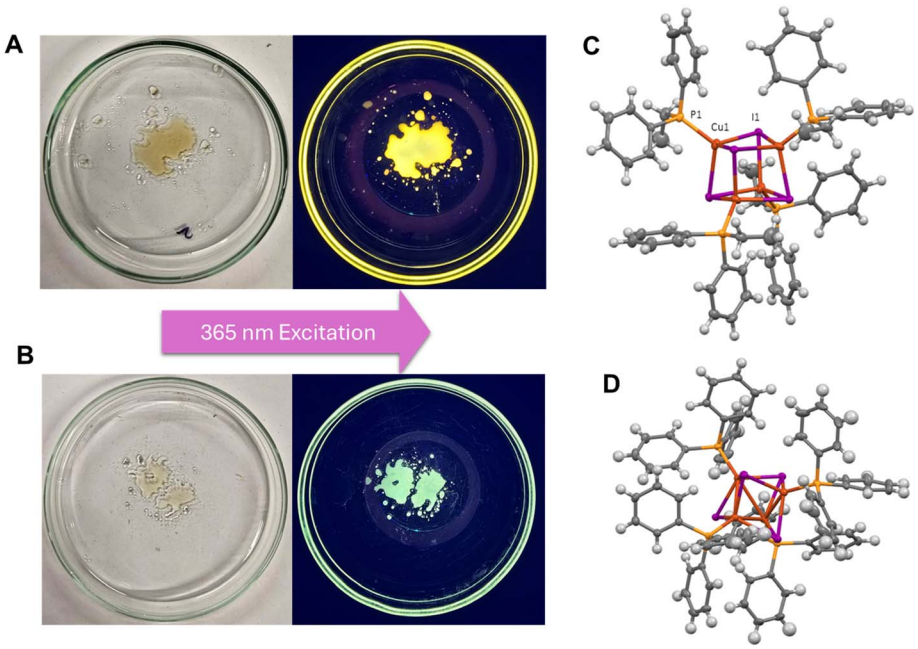

Fig. 1 Top row: melt quenched $[Cu_4I_4(PPh_2Et)_4]$ under ambient light and UV excitation (A) and the corresponding crystal structures of the tetragonal complex (C). Bottom row: melt quenched $[Cu_4I_4(PPh_3)_4]$ under ambient light and UV excitation (B) and the corresponding crystal structures of the monoclinic complex (D), full crystallographic data is presented in Tables S1–S7. Solid state fluorescence images and composites also presented in SI Fig. S2 and S3.

SCXRD data and the previously reported clusters by Dong *et al.* (1). Specifically, the $[Cu_4I_4(PPh_2Et)_4]$ tetragonal polymorph exhibits a known yellow emission maximum at 585 nm, while the monoclinic $[Cu_4I_4(PPh_3)_4]$ exhibits a peak at 570 nm. These values are consistent with the yellow and blue-green fluorescence observed under 365 nm excitation in this study (Fig. 1).

The successful incorporation of copper nanoclusters onto the cellulose acetate film was validated through electron microscopy and spectroscopy. SEM imaging confirmed the formation of granular structures across the polymer surface, distinct from the smoother film and trapped solvent blisters (acetone). Critically, EDX analysis targeted these structures and confirmed they were composed of copper, providing definitive evidence of their successful incorporation. The lack of uniform coating however across the film surface is due to the poor acetone solubility of Cu-PVP, which leads to aggregation of the nanoclusters on the film surface upon solvent casting (Fig. 2). The nanocluster aggregation did not hinder the solid-state fluorescence, but in future trials, nanoclusters with improved acetone solubility should be developed to aid their incorporation in the polymeric film.

$[Cu_4I_4(PPh_3)_4]$ and $[Cu_4I_4(PPh_2Et)_4]$ complexes embedded in melt-quenched glass and Cu-CNAs in cellulose acetate films (CAF) enables UV-to-visible light conversion (SI Fig. 1). Upon excitation at 365 nm, these materials emit strongly at 585 nm (yellow), 570 nm (green) and 410 nm (blue) respectively, wavelengths that align well with the photosynthetically active radiation (PAR) range (SI Fig. 4). These emissions are expected to supplement underutilized portions of the solar spectrum, particularly in greenhouse environments, increasing photon flux in the red and green regions where chlorophyll absorption and light penetration through leaf tissues are most effective. This UV-conversion strategy reduces photodamage while enhancing internal light availability for deeper chloroplast layers, particularly benefiting C_3 crops such as *Raphanus sativus.*

3.2 Spectral-converting composites boosts plant growth and biomass

During the AutoPot trials,[19] all three spectral-film treatments accelerated early leaf expansion between days 7–14 (Fig. 3), with the cellulose-acetate film (CAF; blue emission) and the $[Cu_4I_4(PPh_3)_4]$ composite (blue-green emission) producing the largest early growth benefits. Early blue light is well known to promote stomatal opening and chlorophyll biosynthesis and can therefore stimulate rapid leaf area expansion in developing seedlings.[20–22] This likely explains the statistically significant enhancement in foliar growth observed under the CAF film ($p = 0.046$) in the first 1–2 weeks (Fig. 3). By contrast, between day 14 and harvest the growth advantage shifted: the blue-green $[Cu_4I_4(PPh_3)_4]$ and the yellow $[Cu_4I_4(PPh_2Et)_4]$ composites improved growth rates by 10% and 14% respectively compared to control, whereas the CAF film treatment plateaued (Fig. 3). This growth pattern is consistent with wavelength-dependent roles in canopy light use blue light is most effective in initiating leaf development and pigment synthesis, whereas green and red photons penetrate deeper into leaf tissue and the canopy and are most effective for sustained carbon fixation in mature leaves.[6]

Post harvest, all treatments resulted in increases to harvestable yield. The $[Cu_4I_4(PPh_2Et)_4]$, $[Cu_4I_4(PPh_3)_4]$ and CAF

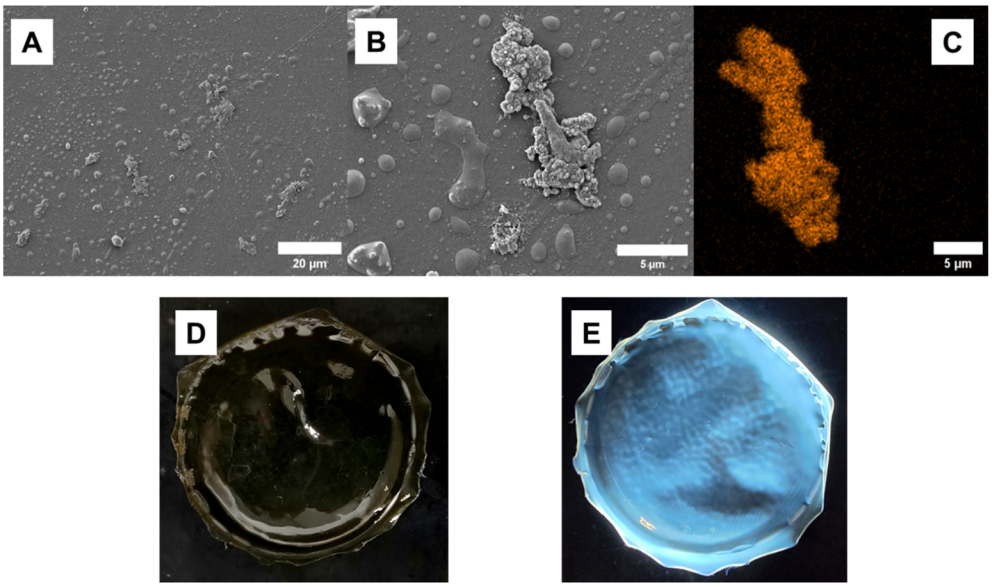

Fig. 2 Top row: SEM imaging confirms the incorporation of Cu-CNAs onto the polymer surface. (A) A wide-field view (1000× mag) shows granular aggregates (*e.g.*, white box) on the film. (B) A higher magnification image (5000× mag) details the morphology of a typical aggregate. (C) The corresponding EDX elemental map for copper confirms that the aggregates are composed of the copper nanoassemblies. Bottom row: photographs showing the flexible composite film under ambient light (D) and its strong, uniform blue photoluminescence (SI Fig. S1) at 410 nm when excited by 365 nm UV light (E).

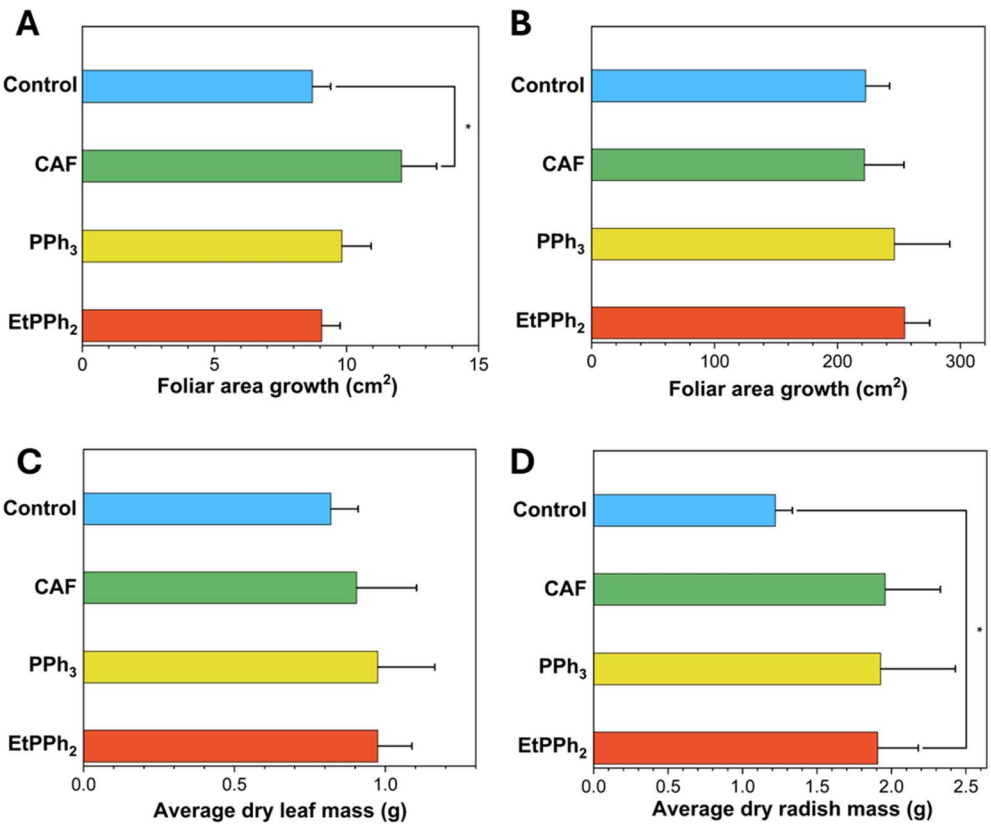

Fig. 3 Effect of spectral-converting composites on the growth and biomass of *Raphanus sativus*. (A) Foliar area growth during the early growth phase (days 7–14). (B) late growth phase days 14- harvest (day 32). Bottom row displays the average dry biomass for leaves (C) and radishes (D) at harvest. Treatments are control, cellulose acetate film (CAF), $[Cu_4I_4(PPh_3)_4]$ (PPh_3), and $[Cu_4I_4(PPh_2Et)_4]$ ($EtPPh_2$). Error bars represent the standard error of the mean for $n = 8$ biological replicates within the treatment pot. An asterisk (*) indicates a significant difference ($p^* < 0.05$) from the control. For plot A $p = 0.046$ for CAF, and in plot D $p = 0.044$ for ($EtPh_2P$).

Table 1 Comparison of the average photosynthetic pigment and ascorbic acid concentrations for *Raphanus sativus* under the fluorescent composite treatments. All data are reported with the average ± standard deviation of the mean ($n = 8$)

Materials	Average normalised carotenoid (mg L^{-1})	Average normalised chlorophyll (mg L^{-1})	Average normalised ascorbic acid (mg L^{-1})
Control	2.50 ± 0.07	14.5 ± 0.40	355 ± 10
$[Cu_4I_4(PPh_2Et)_4]$	2.84 ± 0.12	15.4 ± 0.70	363 ± 16
$[Cu_4I_4(PPh_3)_4]$	2.11 ± 0.11	13.1 ± 1.04	281 ± 13
CAF	2.56 ± 0.14	14.9 ± 1.03	252 ± 19

treatments increased dry foliar mass by 19%, 19% and 10% respectively. Furthermore, the $[Cu_4I_4(PPh_2Et)_4]$ film produced the only treatment to yield a statistically significant increase (56%) in radish average dry mass (1.91 ± 0.77 g), whilst, $[Cu_4I_4(PPh_3)_4]$ and CAF treatments also displayed increases of 58% (1.93 ± 1.42 g) and 60% (1.96 ± 1.05 g) respectively compared to the control (1.22 ± 0.32 g). The usage of the $[Cu_4I_4(PPh_2Et)_4]$ composite also produced the largest increases in chlorophyll, carotenoids and ascorbic acid content compared to the control, however these did not reach the threshold for statistical significance ($p > 0.05$) (Table 1). The yellow emission of $[Cu_4I_4(PPh_2Et)_4]$ (585 nm, λ_{ex} 355 nm) overlaps with the broader absorption spectra of chlorophylls and accessory pigments. While this wavelength does not coincide with the primary absorption peaks of chlorophyll a, it aligns with a region of relatively high quantum yield for CO_2 assimilation. It is possible that since yellow-green photons can penetrate further into the leaf mesophyll compared to blue or red light (6), photosynthesis can be enhanced in lower chloroplast layers that are typically light-limited, which may enhance the biomass accumulation. The elevated carotenoid content under $[Cu_4I_4(PPh_2Et)_4]$ may reflect both increased light harvesting and a demand for photoprotection under higher photosynthetic throughput.[23] By contrast, the CAF and PPh_3 composites, which shift more energy into blue or blue-green wavelengths, supported chlorophyll accumulation (CAF > control) but did not translate into the same statistically significant for harvestable root biomass as $[Cu_4I_4(PPh_2Et)_4]$. Differences in foliar ascorbic acid between treatments may also be spectrum dependent. The ascorbic acid biosynthesis and turnover are responsive to both high-energy (UV/blue) exposure and overall redox load, so treatments that change the balance of blue *vs.* red photons, or that fail to supply additional red flux, can plausibly alter ascorbic acid concentration.

4 Conclusion

This study demonstrates that copper-based luminescent composites can be strategically employed to enhance plant growth and productivity by reshaping the spectral quality of incident light. By converting underutilized UV radiation into targeted regions of the photosynthetically active spectrum, these materials enable wavelength-specific physiological responses that evolve across plant developmental stages. Blue- and blue-green emitting composites preferentially stimulated early foliar expansion, while the yellow-emitting $[Cu_4I_4(PPh_2Et)_4]$ glass composite delivered the greatest improvements in harvestable biomass and metabolite accumulation at maturity. This behaviour is consistent with established spectral dependencies of stomatal regulation, pigment biosynthesis, and carbon fixation efficiency.

Importantly, the materials reported here combine optical tunability with practical processability. Melt-quenched copper iodide clusters provide robust, inorganic spectral filters, while flexible polymer-based Cu-CNA films offer lightweight and adaptable alternatives suitable for greenhouse integration. The use of earth-abundant copper further strengthens the sustainability and economic viability of this approach relative to precious metal or rare earth phosphors.

Beyond the specific crop examined, these findings establish a generalizable framework for the rational design of spectral conversion materials tailored to plant developmental stage, crop type, and growth environment. Future work should firstly employ pot-level replication across multiple blocks to further validates these spectra effects whilst accounting for environmental variance between containers. Secondly future studies should focus on improving long-term photostability, engineering dual- or broadband-emission systems, and validating performance across diverse crops and real-world greenhouse settings. Taken together, this work positions copper-based luminescent composites as a promising materials platform for enhancing photosynthetic efficiency, yield, and nutritional quality in sustainable, controlled-environment agriculture.

Conflicts of interest

All authors declare that there are no conflicts of interest.

Data availability

The data supporting this study are available within the article and its supplementary information (SI). Supplementary information: comprehensive crystallographic datasets for the new tetragonal polymorph, solution-state fluorescence spectra, and photographic documentation of the experimental greenhouse setup; spectral overlap mapping of composite emissions with photosynthetic pigment absorption profiles and the specific calculation equations used for biochemical quantification. Additional rawdata underpinning the findings of this work are available from the corresponding author upon reasonable request. See DOI: https://doi.org/10.1039/d5su00947b.

Acknowledgements

We thank the funding support by the Leverhulme Trust (RPG-2022-277). K.T.K thanks Dr Diana Lednitzky for their technical support and guidance on the electron microscope, Robert Clayton for his advice during plant trials and Jason Ralph-Smith, Autopot UK for the collaboration. Financial support from the Royal Society of Chemistry (grant number C23-4364412079) is also gratefully acknowledged. The authors also acknowledge financial support from the Royal Society International Exchange (IEC\NSFC\242089). The authors acknowledge the usage of https://Biorender.com in the graphical abstract.

References

1 J. A. Burney, S. J. Davis and D. B. Lobell, *Proc. Natl. Acad. Sci. U. S. A.*, 2010, **107**, 12052–12057.
2 E. Kaiser, K. Weerheim, R. Schipper and J. A. Dieleman, *Sci. Hortic.*, 2019, **249**, 271–279.
3 S. J. Mohamed, H. Z. Rihan, N. Aljafer and M. P. Fuller, *Plants*, 2021, **10**, 2162, DOI: 10.3390/plants10102162.
4 S. Mathur, R. Bheemanahalli, S. H. Jumaa, N. Kakar, V. R. Reddy, W. Gao and K. R. Reddy, *Front. Plant Sci.*, 2024, **15**, 1369397, DOI: 10.3389/fpls.2024.1369397.
5 K. J. McCree, *Agric. Meteorol.*, 1971, **9**, 191–216.
6 J. Liu and M. W. van Iersel, *Front. Plant Sci.*, 2021, **12**, 619987, DOI: 10.3389/fpls.2021.619987.
7 S. Muneer, E. Kim, J. Park and J. Lee, *Int. J. Mol. Sci.*, 2014, **15**, 4657–4670.
8 J. Li, G. Li, H. Wang and X. W. Deng, *Phytochrome Signaling Mechanisms. Arabidopsis Book*, 2011, 9, DOI: 10.1199/tab.0148.
9 Z. Bian, X. Zhang, Y. Wang and C. Lu, *Environ. Exp. Bot.*, 2019, **167**, 103844, DOI: 10.1016/j.envexpbot.2019.103844.
10 Z. Bian, Y. Wang, X. Zhang, S. Grundy, K. Hardy, Q. Yang and C. Lu, *Front. Plant Sci.*, 2021, **12**, 649283, DOI: 10.3389/fpls.2021.649283.
11 R. Utrera-Melero, F. Massuyeau, C. Latouche, F. Camerel and S. Perruchas, *Inorg. Chem.*, 2022, **61**, 4080–4091.
12 T. Sasikumar and M. Ilanchelian, *Luminescence*, 2021, **36**, 326–335.
13 C. Shao, S. Xiong, X. Cao, C. Zhang, T. Luo and G. Liu, *Microchem. J.*, 2021, **163**, 105922, DOI: 10.1016/j.microc.2021.105922.
14 C. Dong, X. Song, B. E. Hasanov, Y. Yuan, L. Gutiérrez-Arzaluz, P. Yuan, S. Nematulloev, M. Bayindir, O. F. Mohammed and O. M. Bakr, *J. Am. Chem. Soc.*, 2024, **146**, 7373–7385.
15 G. M. Sheldrick, *Acta Crystallogr., Sect. A: Found. Adv.*, 2015, **71**, 3–8.
16 G. M. Sheldrick, *Acta Crystallogr., Sect. C: Struct. Chem.*, 2015, **71**, 3–8.
17 O. V. Dolomanov, I. J. Bourhis, R. J. Gildea, J. A. K. Howard and H. Puschmann, *J. Appl. Crystallogr.*, 2009, **42**, 339–341.
18 C. F. Macrae, I. Sovago, S. J. Cottrell, P. T. A. Galek, P. McCabe, E. Pidcock, M. Platings, G. P. Shields, J. S. Stevens, M. Towler and P. A. Wood, *J. Appl. Crystallogr.*, 2020, **53**, 226–235.
19 Autopot UK Watering Systems, https://autopot.co.uk/, accessed August 2025.
20 M. Doi, Y. Kitagawa and K. I. Shimazaki, *Plant Physiol.*, 2015, **169**, 1205–1213.
21 S. I. Inoue and T. Kinoshita, *Plant Physiol.*, 2017, **174**, 531–538.
22 Y. Li, G. Xin, L. Liu, Q. Shi, F. Yang and M. Wei, *BMC Plant Biol.*, 2020, **20**, 318, DOI: 10.1186/s12870-020-02523-z.
23 Y. Xu and P. J. Harvey, *Antioxidants*, 2019, **8**, 123, DOI: 10.3390/antiox8050123.